Journal of Contaminant Hydrology 145 (2013) 10–16

Contents lists available at SciVerse ScienceDirect

Journal of Contaminant Hydrology

journal homepage: www.elsevier.com/locate/jconhyd

Experimental study of solute dispersion in macroscopic suspension flow

Y.L. Roht, A. Boschan *, I. Ippolito, R. Chertcoff

Grupo de Medios Porosos, Facultad de Ingeniería, Universidad de Buenos Aires, Paseo Colón 850, 1063, Buenos Aires, Argentina

ARTICLE INFO

Article history:
Received 16 August 2012
Received in revised form 5 November 2012
Accepted 8 November 2012
Available online 19 November 2012

Keywords:
Suspension
Dispersion
Solute
Transport
Particles
Flow

ABSTRACT

We experimentally investigate the influence of suspended neutrally-buoyant particles on the dispersion of a passive solute in pressure-driven axial flow in a constant aperture fracture (parallel plates configuration). A dye is employed as solute in order to measure its local concentration by means of a light transmission technique. In the experiments a dyed particle suspension displaces a transparent one at constant flow rate, for volume fractions ϕ ranging from 0 to 0.25 and for solute Péclet numbers (Pe_s) between 35 and 476 (mean flow velocities U between 0.004 and 0.0544 cm/s). The local time variation of the solute concentration in the measurement zone was well-fitted by the solution of the advection–dispersion equation, and a longitudinal dispersion coefficient D for the solute was measured. For $Pe_s<300$, the values of D for flow with particles ($\phi>0$) and without particles ($\phi=0$) are equal within the measurement error. For $Pe_s>300$, D decreases for $\phi>0$ compared to $\phi=0$. The magnitude of the reduction increases as ϕ increases, and also as Pe_s increases. This decrease of D in the presence of suspended macroscopic particles is analyzed in the light of theoretical, numerical and experimental results from other authors that studied suspension flow in similar geometries.

1. Introduction

The study of transport and dispersion properties in underground formations or structures is of interest in several applications such as safe management of nuclear waste, exploitation of hydrocarbon reservoirs and geothermal heat storage.

Solute dispersion corresponds to the spreading of an initially localized solute concentration distribution due to the combined effects of molecular diffusion and the spatial variations in the flow velocity field.

In subsurface formations two main factors influence solute dispersion:

1) The geometry of the confining media, in which the flow takes place.
2) The mechanical and molecular properties of the flowing material (solvent and solute).

The first factor has been studied extensively by addressing the description of heterogeneity in fractured and porous media, using multiscale and stochastic approaches (Bouchaud, 2003; Gelhar, 1993). Heterogeneity strongly influences the velocity field of the flow and then the dispersion process, for example by generating preferential flow paths or flow anisotropy (Auradou et al., 2006; Yeo et al., 1998) that affect the transit times of the solute. The second factor influences mainly the relative distribution of velocities in the flow, though indirectly affecting solute dispersion (for example by affecting the efficiency of molecular diffusion).

These two factors may interact in a way that can be non-trivial to determine, because the properties of the flowing material may influence dispersion in a different way depending on the confining geometry.

When comparing, for instance, a shear-thinning polymer solution with a Newtonian fluid like water, Taylor dispersion is reduced in parallel plates or capilar geometries because the velocity profile is flattened and tends to be plug-like (Boschan et al., 2003; Vartuli et al., 1995). This flattening is due to the fact that, for a shear-thinning fluid, viscosity is greater in the low shear zones (center of the gap) and smaller

* Corresponding author. Tel.: +54 1143430891.
E-mail address: aboschfi@gmail.com (A. Boschan).

0169-7722/$ – see front matter © 2012 Elsevier B.V. All rights reserved.
http://dx.doi.org/10.1016/j.jconhyd.2012.11.003

in the high shear zones (near the walls). On the other hand, geometrical dispersion and macrodispersion in porous media and variable aperture fractures are enhanced, because velocity contrasts between different flow paths are increased (Auradou et al., 2008; D'Onofrio et al., 2002; Shah and Yortsos, 1995).

Moreover, in many cases of subsurface and industrial flows, the solvent may carry macroscopic solid particles in suspension in addition to the solute. The behavior of a flowing suspension may be much more complex than that of a homogeneous fluid due to fluid–particle or particle–particle interactions, that may lead to particle concentration gradients and relative motion between particles and fluid. Particles may organize or migrate changing locally the properties of the flow. As a consequence, the transport of, for example, a dissolved contaminant, may be hard to predict. This raises a fundamental interest in understanding solute dispersion in suspension flow.

While spreading and dispersion of solutes in fluid flow have been the subject of research for many years, it is quite recently that systematic studies of the flow properties of particle suspensions have been performed, mainly because of its relevance to a wide range of industrial and environmental applications (food and personal care industries, drilling fluids, sediment transport in rivers, lakes and irrigation channels), and also because new experimental and numerical techniques have been developed (Matas et al., 2004). Suspension flow and rheology is indeed currently a subject of intense research (Deboeuf et al., 2011; Ovarlez et al., 2006).

To our knowledge very few works have addressed the issue of solute dispersion in suspension flow. Motivated by groundwater contamination Massei et al. (2002) studied experimentally the transport and deposition of quartz particles of approx. 25 μm in a highly permeable porous media. They found a retardation of the solid phase with respect to the dissolved phase (fluorescein), and measured a higher dispersivity for the latter. Zheng et al. (2009) studied numerically the differential transport and dispersion of colloid particles and molecular scale solutes in constant and variable aperture fractures, finding the conditions for which Taylor dispersion can describe accurately colloid dispersion.

The objective of the present work is to study experimentally how the presence of macroscopic particles in the flow affects the dispersion of the solute. The organization of this work is as follows. We first introduce the topics of solute dispersion in Newtonian and non-Newtonian fluids, and then we describe some of the mechanisms related to suspension flow. We then present the experimental methodology and setup, followed by the data processing techniques. Finally the results are discussed and conclusions are presented.

1.1. Solute dispersion in Newtonian fluids

In the absence of flow, solute dispersion is due mostly to molecular diffusion. When flow exists, dispersion is due to the combined effects of the molecular diffusion and the spatial variations of the flow velocity. In many situations, for example in media with weak and uniformly distributed permeability fluctuations, the variation of the solute concentration C satisfies the classical macroscopic advection–dispersion equation (Bear, 1972):

Moreover, in the case of simple flow geometries (infinite parallel plates (pp), cylindrical tubes (ct)) such as the one studied in this work, the variation of the longitudinal dispersion coefficient with the mean flow velocity is given by Eq. (1) (Aris, 1956; Golay, 1958).

$$\frac{D}{D_m} = 1 + \mathrm{Pe}_s^2 f; \quad \left(f_{pp} = 1/210; f_{ct} = 1/48\right); \qquad \mathrm{Pe}_s = \frac{dU}{D_m}; \quad (1)$$

where d is the typical distance across the flow, U is the mean flow velocity and D_m is the molecular diffusion coefficient. The Péclet number of the solute, Pe_s, characterizes the relative influence of the molecular diffusion of the solute and of its advective transport. A distinction should be made with respect to the particle Péclet number Pe_p that will be introduced in Section 1.3.

In more complex geometries, geometrical dispersion and macrodispersion (Roux et al., 1998) may exist due to the effect of heterogeneity on the flow.

1.2. Solute dispersion in non-Newtonian fluids

Non-Newtonian fluids include oil, blood, polymers and gels. In non-Newtonian flow, the relative distribution of velocities in the flow is likely to be modified compared to Newtonian flow. This may affect solute dispersion mechanisms as explained in the previous section. The effects of fluid rheology on dispersion have been for example investigated using shear-thinning polymer solutions both in simple flow geometries (in parallel plates or capilar tubes) (Boschan et al., 2003; Vartuli et al., 1995), variable aperture fractures (Boschan et al., 2007, 2008) and in porous media (D'Onofrio et al., 2002; Fadili et al., 2002). In general, for these solutions, the viscosity is maximal for low shear rates and decreases with increasing shear rate, yielding frequently flat, plug-like, velocity profiles. This behavior is usually described by the use of power-law and truncated power-law models.

Moreover, the Taylor dispersion coefficient D for the flow of a power-law fluid can be calculated analytically for flow in parallel plates (pp) or in cylindrical tubes (ct) (Boschan et al., 2003; Vartuli et al., 1995):

$$\frac{D}{D_m} = 1 + \mathrm{Pe}_s^2 f(n); \quad f(n)_{pp} = \frac{n^2}{6(2+5n)(1+4n)}, \qquad (2)$$
$$f(n)_{ct} = \frac{n^2}{2(1+3n)(1+5n)}$$

where n is the rheological index of the fluid in the power law model ($n=1$ for Newtonian fluids). For shear-thinning fluids $n<1$ and then $f(n)<f(n=1)$, implying a reduction of D compared to the Newtonian case. This reduction is mainly due to the flattening of the velocity profile mentioned before.

1.3. Suspension flow: mechanisms of interaction

The particle Péclet number $\frac{\mathrm{Pe}_p = 6\pi\mu_0 a^3\dot{\gamma}}{kT}$ and the particle Reynolds number $\frac{\mathrm{Re}_p = \rho_0 a^2\dot{\gamma}}{\mu_0}$ account for the relative magnitude of viscous and Brownian effects, and of inertial and viscous effects respectively (here a is the particle radius, $\dot{\gamma}$ the characteristic shear-rate, ρ_0 the density of the particle, μ_0 the

viscosity of the solvent, k Boltzmann's constant, and T the absolute temperature). In this work we consider only macroscopic non-Brownian suspensions, and negligible inertial effects (such as the inertial particle migration (Segré and Silberberg, 1962)). This situation corresponds to very high Pe_p and very low Re_p limit (we estimate the values of both for our experiments in Section 5).

In these conditions, fluid–particle and particle–particle interactions are then mostly driven by viscous stresses. Lately, the phenomena of shear-induced diffusion and shear-induced particle migration have been of interest. A first experimental observation was reported by Eckstein et al. (1977), and later studied by many authors from the theoretical and experimental point of view (Leighton and Acrivos, 1987; Lyon and Leal, 1998; Phillips et al., 1992). The net migration of the particles caused by this mechanism (Nott and Brady, 1994) can induce inhomogeneities of the particle concentration, which can in turn strongly affect the velocity field.

In the following, we investigate experimentally the possible influence of the features discussed above on passive solute dispersion.

2. Materials and methods

2.1. Fluid and suspension preparation

The preparation of the suspensions was performed in order to achieve neutral buoyancy of the particles: the carrier fluid is a Newtonian solution containing 21% by weight of glycerol in water (approx. 1.05 g/cm^3).

This solution is fractioned in two equal parts, then the solute (WaterBlue dye, Horobin and Kiernan, 2002) is added to one part (2.0 g/l), while NaCl is added to the other (2.0 g/l). This is done in order to match densities and avoid gravity-driven instabilities between the carrier fluids of the dyed displacing suspension and the transparent displaced suspension. A small amount of SDS surfactant is added to each part in order to improve the wettability; finally an identical quantity of spherical particles (Dynoseeds TS40, diameter: 40 ± 2 μm, density: 1.05 g/cm^3) is added to each part in order to obtain the desired ϕ.

Whenever the preparation yielded suspensions that were visibly not neutrally-buoyant, corrections were applied by adding small drops of water or glycerol simultaneously to both dyed and transparent fractions. The suspensions were left in observation in a cylindrical elongated bottle for 3 days before performing the experiments. This is done in order to avoid significant vertical buoyant displacement during the experiments. We estimate that the presence of a layer of clear fluid at the top or at the bottom of the suspension could be determined with reasonable accuracy and by direct inspection if the layer has at least a thickness of 0.5 cm. A displacement of 0.5 cm in 3 days would correspond to a displacement of 0.007 cm (a sixth of the measured fracture aperture d, cf. Section 2.2) in the typical duration of our longest experiments (1 h).

The absence of such a layer suggests that the vertical buoyant displacement of the particles during all the experiment is at most smaller than a sixth of the fracture aperture in the longest experiments. In addition very few particles were observed attached to either fracture wall at the end of the experiment. The room temperature was controlled during preparation of suspensions and during the experiments in order to avoid temperature-related density effects.

Suspensions were prepared with volume fractions ϕ equal to 0.05, 0.1, 0.15, 0.2, and 0.25.

2.2. Experimental device and procedure

The constant aperture fracture was constructed using two rectangular, parallel and horizontal flat glass plates (25 cm × 10 cm × 1 cm). Two narrow mylar strips (25 cm × 1 cm × 0.035 cm) provided a constant separation between the two plates and sealed the longest sides of the fracture (see Fig. 1). In this way, an axial flow was established between the inlet and outlet (two shorter sides of the fracture). The inlet side was attached to a fluid reservoir with an open top; the outlet was connected to a syringe pump sucking the suspensions out of the fracture at a constant flow rate.

In this work, a transparent suspension, initially saturating the fracture, is displaced by a dyed suspension, until complete saturation. The experimental procedure for the displacement experiments (initial saturation of the fracture, obtention of a straight sharp initial displacement front between the transparent and dyed suspensions, etc.) is identical to that reported in Boschan et al. (2007, 2008). Images of the transmitted light intensity in all the fracture were acquired at constant time intervals. The fracture aperture d was estimated from a comparison between the pump flow rate and the measured values of U, yielding 0.042 ± 0.001 cm.

For $\phi = 0.05$, 0.1, and 0.2, displacement experiments of suspensions were performed at mean flow velocities ranging between 0.004 and 0.0544 cm/s (leading to $35 < Pe_s < 476$). Depending on Pe_s, the duration of the experiments required to record the complete saturation of the fracture ranged between 10 min and 2 h (time interval between 6 s and 76 s, with a total of 100 acquired images in each experiment).

For $350 < Pe_s < 450$ we detected a significant difference in the solute dispersion coefficient values for $\phi > 0$ compared to $\phi = 0$: we studied this range of Pe_s in detail, by performing three similar experiments for each ϕ and Pe_s. In this case experiments were performed also for $\phi = 0.05$, 0.1, 0.15, 0.2, and 0.25.

As a complement to the displacement experiments with suspensions, we performed also a number of auxiliary experiments using exactly the same device assembly.

1) Anytime a displacement experiment for $\phi > 0$ was performed, a reference experiment ($\phi = 0$) was also performed, at the same flow rates. This procedure allowed us to compare experiments with and without suspended particles, while keeping all the other experimental parameters constant.
2) For each series of displacement experiments for a given ϕ (> 0), a light transmission calibration was performed using pattern suspensions with six different dye concentrations but with the same ϕ. This procedure allowed us to obtain, for each ϕ, a calibration curve that relates locally the dye concentration to the transmitted light intensity.
3) A light transmission calibration specifically for $\phi = 0$, in order to process the reference experiments.

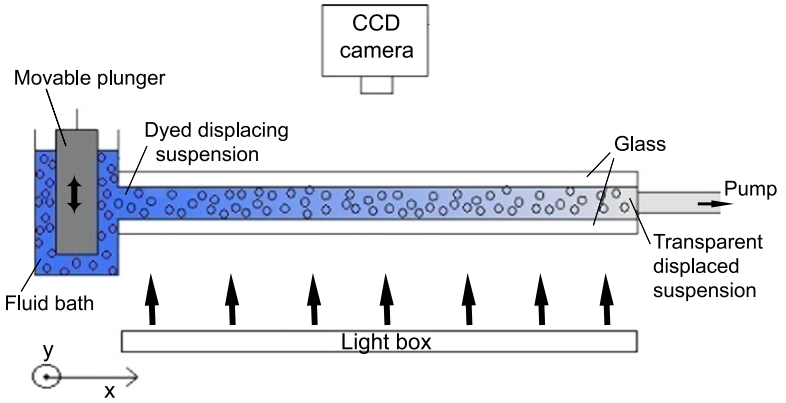

Fig. 1. Schematic view of the experimental setup. The dyed suspension displaces the transparent one at constant flow rate.

3. Image processing and data analysis

The measurement zone in the acquired images was chosen in order to assure that the Taylor regime had been achieved: given the characteristic time of transverse solute molecular diffusion $\tau_d = (d/2)^2/D_m$ and of solute advection $\tau_a = X_m/U$, the Taylor regime may be considered achieved for a given X_m if the former time is significantly smaller than the latter. If so, the transverse molecular diffusion had time enough to homogenize the solute concentration in the direction perpendicular to the flow. Here U is the mean flow velocity, D_m the solute molecular diffusion coefficient ($4.8\ 10^{-6}$ cm^2/s), X_m is the longitudinal position in the flow direction, and d is the fracture aperture.

With this criterion, and considering, for instance, one of our experiments with $Pe_s = 450$ ($U = 0.0514$ cm/s), the above condition is satisfied near the outlet ($X_m = 25$ cm), having $\tau_d = 92$ s and $\tau_a = 486$ s. The Taylor regime can be then considered achieved in this case.

We then chose to set a rectangular measurement zone of dimensions 7.4 cm (x) by 4.6 cm (y) located near the outlet of the fracture, starting 14.7 cm from the fracture inlet. The transmitted intensity values for each pixel at position (x,y) in the measurement zone is converted to local solute concentration $C(x,y)$ values by using the light transmission calibration. For further details on the light transmission technique we refer to Boschan et al. (2007, 2008).

The time variation $C(x,y,t)$ is then fitted, for each (x,y), using Eq. (3) (which is the solution of the advection–dispersion equation) in order to obtain a transit time $T_0(x,y)$ and a coefficient of dispersion $D(x,y)$ (here C_0 is the dye concentration of the dyed suspension).

$$\frac{C}{C_0} = \frac{1}{2}\left[\left(1 - \mathrm{erf}\left(\frac{T_0 - t}{2\sqrt{tD/U^2}}\right)\right)\right] \tag{3}$$

In all experiments T_0 varied linearly with measuring positions indicating that U is constant with time. Finally, in a first method, from the spatial distribution of $D(x,y)$ values, and in the given measurement zone, we obtained the Taylor dispersion coefficient as $D = \langle D(x,y)\rangle_{x,y}$ and its error $\Delta D = \sigma_{x,y}(D)/2$ for each experiment (the error bars presented in the results correspond to ΔD). A second method in which D is obtained from the slope of the variation of the square deviation of the concentration distribution Δt^2 with T_0 (we refer to Boschan et al. (2003) for a detailed description of this method) allows us to cross check the results. Moreover, in this second method the value of D obtained is independent of any possible unavoidable mixing when the displacing and displaced suspensions are put in contact.

Fig. 2 shows the time variation of $C(x,y,t)$, normalized by C_0 and the fit with the ADE solution of Eq. (3) performed in order to obtain D. In the measurement zone, D reaches a constant value (inset). This is consistent with the relationship between diffusive and advective characteristic times, and shows that the Taylor regime has been achieved.

In test experiments for Pe_s higher than 500, the time variation of the concentration in the measurement zone (or even for x very close to the outlet) was not well fitted by a Gaussian function, meaning that the fracture used is not long enough in order for the Taylor regime to be achieved. Therefore Pe_s values higher than 500 were not investigated.

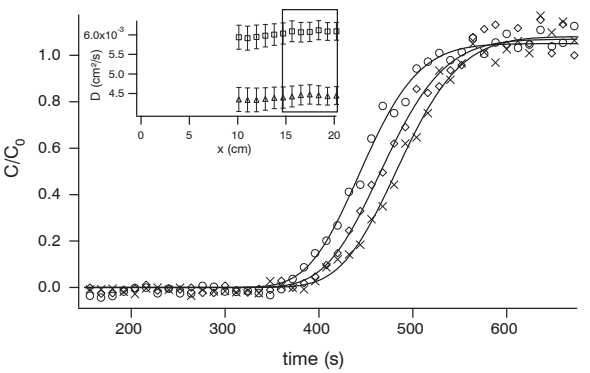

Fig. 2. Symbols: time variation of the normalized dye concentration $c(x,y,t)$ for three different positions x located in the center of the fracture width, at distances 16.5 cm (○); 17.5 cm (◇); and 18.5 cm (X) from the inlet. Full line: Datafit with the solution of the advection–dispersion equation. Inset: variation of the average $\langle D(x,y)\rangle_{x,y}$ as a function of the distance x from the fracture inlet. (□): $\phi = 0$; (Δ): $\phi = 0.2$; $Pe_s = 450$. The rectangle shows the range of x corresponding to the measurement zone chosen.

4. Results

In this section we present results concerning the dependence of D on ϕ and on Pe_s. Fig. 3 shows the variation of D with Pe_s particles for all the range of Pe_s studied. For low values of Pe_s, no significant difference can be observed between different values of ϕ. As Pe_s increases, the values of D decrease for $\phi>0$ compared to $\phi=0$. This relative decrease is greater for increasing ϕ.

The difference between the theoretical prediction for the infinite parallel plates configuration and the reference measurements (both for $\phi=0$) may be due to the finite ratio between fracture aperture and width in our experiments. It has been shown theoretically (Chatwin and Sullivan, 1982) that such a finite ratio increases the value of D relatively to the infinite parallel plates configuration (infinite width).

We must take in account that the Taylor regime may not be achieved along the wider direction of the fracture (width = 8 cm) in a 25 cm long fracture (cf. Section 3). Hence, the prediction of a factor ~7 from Chatwin and Sullivan (1982) do not exactly apply in our current experiments. However, even if the Taylor regime is not achieved (for example in advective conditions), we can still assume that the finite ratio between fracture aperture and width modifies the infinite parallel plates value of D by increasing it by a factor larger than 1, as measured by us.

The magnitude of the relative decrease mentioned above is shown in Fig. 4. This figure shows the variation of the ratio $D/D(\phi=0)$ (D divided by the reference value without particles) for $350<Pe_s<450$. While for $\phi=0.05$ and $\phi=0.1$ the values of D seem unaffected by the presence of particles, the decrease is evident for $\phi=0.2$ and $\phi=0.25$, reaching approx. 20% on average and a maximum of 26% for $Pe_s=450$ ($\phi=0.2$; 0.25).

Fig. 5 shows the variation of the dispersivity $l_d=D/U$ with Pe_s. For $Pe_s<300$, l_d increases approximately linearly with Pe_s for all values of ϕ in accordance with the quadratic dependence of D with Pe_s from Eq. (1). In particular, the values of l_d for $\phi=0$ and $\phi>0$ follow the same linear trend.

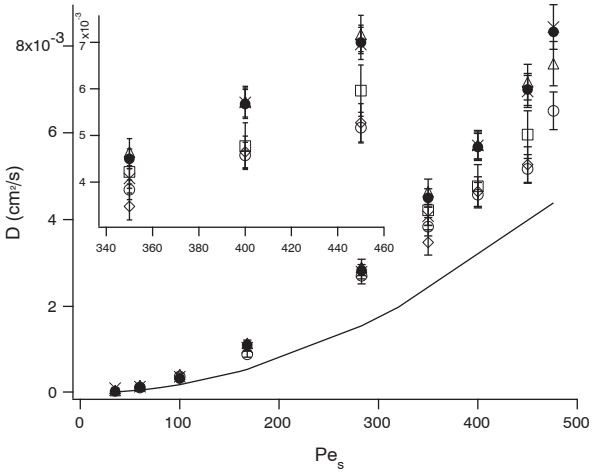

Fig. 3. Dispersion coefficient D as a function of Pe_s. (●): $\phi=0$ (reference experiments); (X): $\phi=0.05$; (Δ): $\phi=0.1$; (□): $\phi=0.15$; (○): $\phi=0.2$; (◇): $\phi=0.25$. Full line: theoretical prediction for infinite parallel plates ($\phi=0$) (see Section 1.1). Inset shows a zoom for $350<Pe_s<450$.

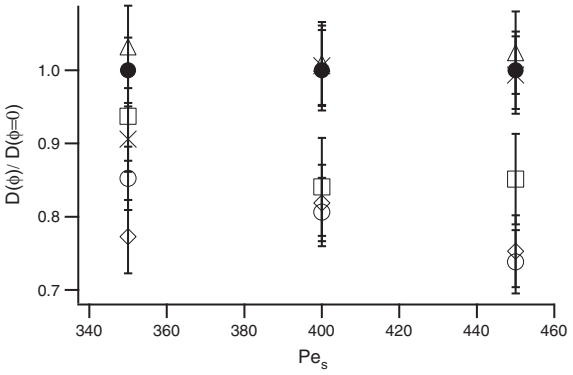

Fig. 4. Ratio of D measured for suspensions ($\phi>0$) to D measured for reference experiments ($\phi=0$) as a function of Pe_s. (●): $\phi=0$ (reference experiments); (X): $\phi=0.05$; (Δ): $\phi=0.1$; (□): $\phi=0.15$; (○): $\phi=0.2$; (◇): $\phi=0.25$.

For $Pe_s>300$, this trend continues if $\phi<0.15$, but, for $\phi>0.15$, l_d decreases markedly.

5. Discussion and conclusions

The results shown in the previous section evidence that, for $Pe_s>300$ and for $\phi>0.15$, the presence of the particles in suspension may affect solute dispersion by reducing the longitudinal dispersion coefficient.

Given the mean distance between the center of the particles (of order 10^2 μm, depending of the volume fraction ϕ), the molecular diffusion D_m of the solute in the carrier fluid should not be altered by the presence of the particles. It has indeed been shown in previous works (Vartuli et al., 1995) that the much smaller polymer chains would not significantly modify D_m and that its value can be considered unaltered compared to its value in water. Although the influence of an increased tortuosity should not be completely disregarded, the above argument from previous works suggests that the explanation for the decrease of dispersion observed should be sought mainly on the modification of the velocity field introduced by the presence of particles in suspension. Regarding possible Brownian or inertial effects, with the definitions of Section 1.3, for our experiments we obtain $Pe_p=2.18\ 10^5$ and $Re_p=0.0067$ ($\mu_0=1{,}6$ cP, $a=2\ 10^{-5}$ m, $\dot{\gamma}=U_{max}/(d/2)=3{,}6$ 1/s, $T=293$ K, $\rho_0=1{,}05$ g/cm^3). In these conditions both effects can be reasonably neglected.

Several experimental (Hampton et al., 1997; Koh et al., 1994); and theoretical (Nott and Brady, 1994; Yapici et al., 2009) studies of suspension flow have reported, for small values of Re_p, a flattening (or blunting) of the velocity profile compared to the parabolic Poiseuille profile of Newtonian fluids. These authors also found this effect to be stronger with increasing ϕ.

This phenomenon has been explained (Nott and Brady, 1994), in the limit of vanishing Re_p, by means of a shear-induced diffusion mechanism (introduced in Section 1.3), which makes the particles migrate towards low shear zones (i.e. the center of the gap in parallel-plate geometry), increasing their concentration there. A constitutive diffusion model developed by Phillips et al. (1992) quantitatively accounts for shear-induced particle migration effects. For flow in a cylindrical tube (shear conditions similar to those in our work) the model predicts

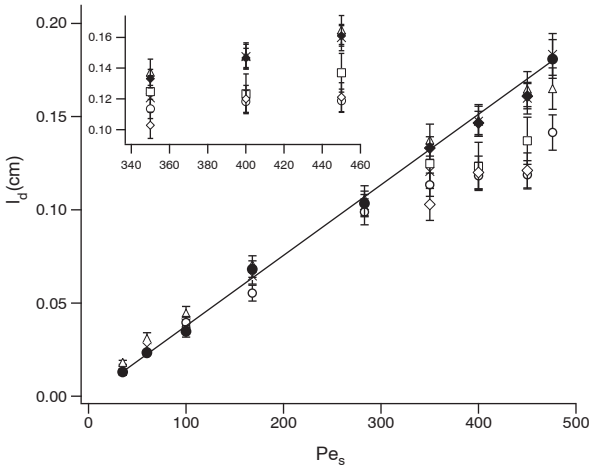

Fig. 5. Dispersivity l_d as a function of Pe_s for all experiments performed. (●): $\phi=0$ (reference experiments); (X): $\phi=0.05$; (Δ): $\phi=0.1$; (□): $\phi=0.15$; (○): $\phi=0.2$; (◇): $\phi=0.25$. Inset shows a zoom for $350<Pe_s<450$. Full line: linear fit for (●).

higher particle concentrations in the center of the tube, and a gradually flattening of the velocity profile with increasing ϕ.

From the mathematical definition of D for an arbitrary velocity profile (Vartuli et al., 1995, equation [5]), a flattening of the latter is related to a decrease in D. From the physical point of view, this is because a flattened velocity profile makes transverse diffusion, and then the overall longitudinal dispersion process, less efficient.

Moreover, in Section 1.2 it was shown quantitatively how, for the specific case of a homogeneous shear-thinning fluid, a flattening of the velocity profile implied theoretically a decrease in D (Boschan et al., 2003; Vartuli et al., 1995). This decrease was also measured experimentally in the latter work. We consider that the decrease of D measured in our experiments could be explained by the flattening of the velocity profile due to shear-induced particle migration.

Regarding length scales, the steady state (flattened) velocity profile due to particle migration is achieved only after a transition length $L/(d/2)$ that scales as $((d/2)/a)^2$ (Nott and Brady, 1994). Here d is the fracture aperture and a the particle radius. In the measurement zone used for analyzing our experiments, $((d/2)/a)^2$ is of order 10^2, and $L/(d/2)$ is of order 10^3, so steady state for the velocity profile can be considered as having been achieved. The choice of the measurement zone requires that the Taylor regime for the solute dispersion (cf. Section 2), and the steady state of the suspension velocity profile, are both achieved simultaneously.

Finally, the validity of a light transmission technique for measuring the solute concentration in suspension flow, such as the one used in this work, should be limited to low values of ϕ, due to the fact that for higher values of ϕ the quantity of light absorbed by the particles may become significant compared to the transmitted one, thus affecting the precision and usability of the technique.

Acknowledgments

We thank J.P. Hulin and H. Auradou for their constructive remarks.

This work was greatly facilitated by CONICET and the CNRS—Conicet International Associated Laboratory LIA-PMF (Physics and Mechanics of Fluids) and by the UBACYT 2002100100798 program.

References

Aris, R., 1956. On dispersion of a solute in a fluid flowing through a tube. Proceedings of the Royal Society of London. Series A 235, 67.

Auradou, H., Drazer, G., Boschan, A., Hulin, J.P., Koplik, J., 2006. Flow channelization in a single fracture induced by shear displacement. Geothermics 35, 576–588.

Auradou, H., Boschan, A., Chertcoff, R., Gabbanelli, S., Ippolito, I., Hulin, J.P., 2008. Enhancement of velocity contrasts by shear thinning solutions flowing in a rough fracture. Journal of Non-Newtonian Fluid Mechanics 153, 53–61.

Bear, J., 1972. Dynamics of Fluids in Porous Media. American Elsevier, New York.

Boschan, A., Charette, J., Gabbanelli, S., Ippolito, I., Chertcoff, R., 2003. Tracer dispersion of non-Newtonian fluids in a Hele Shaw cell. Physica A 327, 49–53.

Boschan, A., Auradou, H., Chertcoff, R., Ippolito, I., Hulin, J.P., 2007. Miscible displacement fronts of shear thinning fluids inside rough fractures. Water Resources Research 43, W03438.

Boschan, A., Ippolito, I., Chertcoff, R., Auradou, H., Hulin, J.P., 2008. Geometrical and Taylor dispersion in a fracture with random obstacles: an experimental study with fluids of different rheologies. Water Resources Research 44, W06420.

Bouchaud, E., 2003. The morphology of fracture surfaces: a tool for understanding crack propagation in complex materials. Surface Review and Letters 10, 797–814.

Chatwin, P.C., Sullivan, P.J., 1982. The effect of aspect ratio on longitudinal diffusivity in rectangular channels. Journal of Fluid Mechanics 120, 347–358.

D'Onofrio, A., Freytes, V.M., Rosen, M., Allain, C., Hulin, J.P., 2002. Echo tracer dispersion in flows of polymer solutions through porous media: a tool for detecting weak permeability heterogeneities? The European Physical Journal E 7, 251–259.

Deboeuf, A., Gauthier, G., Martin, J., Salin, D., 2011. Segregation and periodic mixing in a fluidized bidisperse suspension. New Journal of Physics 13, 075005.

Eckstein, E.C., Bailey, D.G., Shapiro, A.H., 1977. Self-diffusion of particles in shear flow of a suspension. Journal of Fluid Mechanics 79, 191–208.

Fadili, A., Tardy, P., Pearson, A., 2002. A 3D filtration law for power-law fluids in heterogeneous porous media. Journal of Non-Newtonian Fluid Mechanics 106, 121–146.

Gelhar, L.W., 1993. Stochastic Subsurface Hydrology: Englewood Cliffs. Prentice Hall, New Jersey . (390 pp.).

Golay, M.J.E., 1958. Gas Chromatography. Butterworths, London.

Hampton, R.E., Mammoli, A.A., Graham, A.L., Tetlow, N., Altobelli, S.A., 1997. Migration of particles undergoing pressure-driven flow in a circular conduit. Journal of Rheology 41, 621.

Horobin, R.W., Kiernan, J.A., 2002. Conn's Biological Stains: A Handbook of Dyes, Stains and Fluorochromes for Use in Biology and Medicine. Taylor and Francis, Philadelphia, Pa.

Koh, C.J., Hookham, P., Leal, L.G., 1994. An experimental investigation of concentrated suspension flows in a rectangular channel. Journal of Fluid Mechanics 266, 1.

Leighton, D., Acrivos, A., 1987. The shear-induced migration of particles in concentrated suspensions. Journal of Fluid Mechanics 181, 415–439.

Lyon, M.K., Leal, L.G., 1998. An experimental study of the motion of concentrated suspensions in two-dimensional channel flow. Part 2. Bidisperse systems. Journal of Fluid Mechanics 363, 57–77.

Massei, N., Lacroix, M., Wang, H.Q., Dupont, J.P., 2002. Transport of particulate material and dissolved tracer in a highly permeable porous medium: comparison of the transfer parameters. Journal of Contaminant Hydrology 57 (1–2), 21–39.

Matas, J.P., Morris, J.F., Guazzelli, E., 2004. Lateral forces on a sphere. Oil & Gas Science and Technology-Revue De L Institut Francais Du Petrole 59, 59–70.

Nott, P.R., Brady, J.F., 1994. Pressure-driven flow of suspensions: simulation and theory. Journal of Fluid Mechanics 275, 157–199.

Ovarlez, G., Bertrand, F., Rodts, S., 2006. Local determination of the constitutive law of a dense suspension of noncolloidal particles through magnetic resonance imaging. Journal of Rheology 50 (3), 259–292.

Phillips, R.J., Armstrong, R.C., Brown, R.A., Graham, A.L., Abbott, J.R., 1992. A constitutive equation for concentrated suspensions that accounts for shear-induced particle migration. Physics of Fluids A: Fluid Dynamics 4, 30–40.

Roux, S., Plouraboué, F., Hulin, J.P., 1998. Tracer dispersion in rough open cracks. Transport in Porous Media 32, 97–116.
Segré, G., Silberberg, A., 1962. Behaviour of macroscopic rigid spheres in Poiseuille flow Part 2. Experimental results and interpretation. Journal of Fluid Mechanics 14, 136–157.
Shah, C.B., Yortsos, Y.C., 1995. Aspects of flow of power-law fluids in porous media. AICHE Journal 41 (5), 1099–1112.
Vartuli, M., Hulin, J.P., Daccord, G., 1995. Taylor dispersion in a polymer solution flowing in a capillary tube. AICHE Journal 41 (7), 1622–1628.
Yapici, K., Powell, R.L., Phillips, R.J., 2009. Particle migration and suspension structure in steady and oscillatory plane Poiseuille flow. Physics of Fluids 21, 053302.
Yeo, I.W., De Freitas, M.H., Zimmerman, R.W., 1998. Effect of shear displacement on the aperture and permeability of a rock fracture. International Journal of Rock Mechanics and Mining Sciences 35, 1051–1070.
Zheng, Q., Dickson, S.E., Guo, Y., 2009. Differential transport and dispersion of colloids relative to solutes in single fractures. Journal of Colloid and Interface Science 339 (1), 140–151.